

Utilizing Network Properties to Detect Erroneous Inputs

Matt Gorbett¹ Nathaniel Blanchard¹

Abstract

Neural networks are vulnerable to a wide range of erroneous inputs such as adversarial, corrupted, out-of-distribution, and misclassified examples. In this work, we train a linear SVM classifier to detect these four types of erroneous data using hidden and softmax feature vectors of pre-trained neural networks. Our results indicate that these faulty data types generally exhibit linearly separable activation properties from correct examples, giving us the ability to reject bad inputs with no extra training or overhead. We experimentally validate our findings across a diverse range of datasets, domains, pre-trained models, and adversarial attacks.

1. Introduction

Humans are capable of adapting to diverse types of data in ways machine learning models cannot (Geirhos et al., 2018). While the human visual system is able to generalize across varying image representations such as different Instagram filters, deep learning classifiers misbehave when presented with image corruptions (Dodge & Karam, 2017; Hendrycks & Dietterich, 2019), adversarial examples (Szegedy et al., 2014), and previously unseen classes (Bendale & Boulton, 2015; Hendrycks et al., 2019; Scheirer et al., 2013). In this work, we automatically *detect* a broad range of inputs that will be incorrectly classified by a neural network. The timely, preemptive detection of these failures is essential for preventing unreliable AI action based on incorrect predictions. With the deployment of deep learning models in real-world applications such as autonomous vehicles and medical devices, an automated technique that broadly identifies when a model is in error is critically important for safe AI (Amodei et al., 2016).

Erroneous inputs come in many forms, and subsequently much of the research has been siloed into sub-domains. Out-of-distribution detection identifies when inputs are outside of a model’s training (i.e., unseen classes) (DeVries & Taylor, 2018; Hendrycks et al., 2019; Lee et al., 2018; Liang et al., 2018; Scheirer et al., 2013). Adversarial inputs are subtly perturbed examples meant to fool a model (Lu et al., 2017; Metzen et al., 2017; Pang et al., 2018). Corrupted

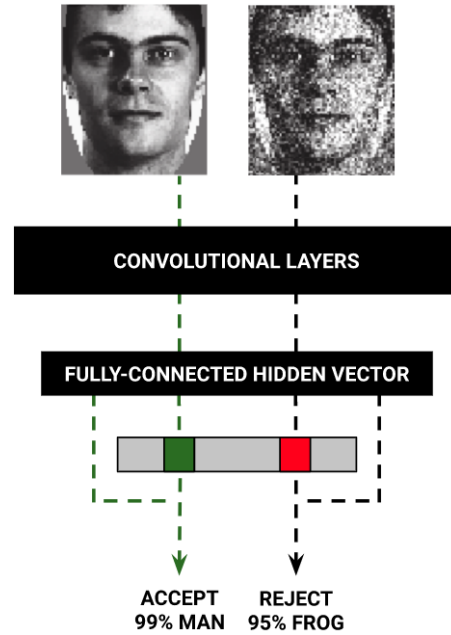


Figure 1. Current neural network models are vulnerable to erroneous inputs (adversarial, corrupted, out-of-distribution, and other misclassifications). We find we can preemptively detect this broad set of inputs from the network’s own internal activations in response to the stimuli. For example, in this figure, an image corrupted by Gaussian noise (which the network will incorrectly classify as a frog) is identified and halted, while the non-corrupted version is allowed to proceed normally. We find we accurately classify erroneous inputs across a range of models and datatypes.

inputs are similar to adversarial examples but are typically not malicious (Hendrycks & Dietterich, 2019). Finally, misclassifications are an inevitable part of any model, as no model has an absolutely perfect performance.

Given the breadth of erroneous input variations, it is unsurprising that each of these inputs has been traditionally tackled as a separate, individual problem requiring a unique, specialized solution. However, in our study of these seemingly disparate phenomena we noticed a common theme: the network’s internal activation patterns were notably distinct when stimuli were *correctly* processed. We hypothesized that, by broadly considering inputs to be either “correctly” or “incorrectly” processed, we could detect erroneous examples across a broad range of inputs.

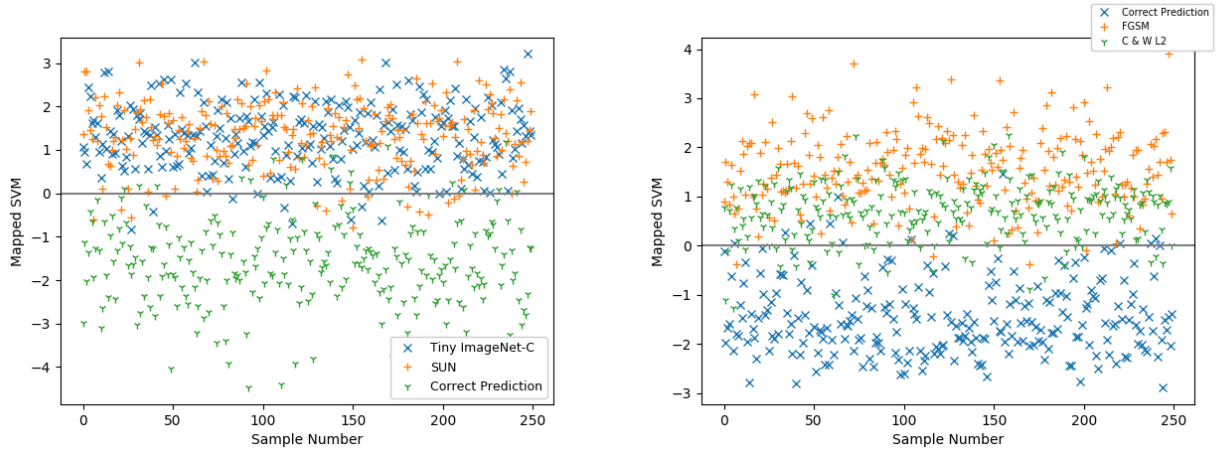


Figure 2. Two graphs showing the linear separability of erroneous datasets from correctly classified examples for the Tiny ImageNet model. "0" on the y-axis represents the optimal hyperplane in a linear SVM classifier. Left: Corrupted (Tiny ImageNet-C) and out-of-distribution images (SUN) are separated from correctly classified images using the sorted softmax features. Right: Two adversarial attack methods, FGSM and Carlini and Wagner l_2 , are separated from correctly classified inputs using the activations of the final hidden layer. Ultimately, we combined these features to achieve state-of-the-art results (Section 4.2). We include only the first 250 examples from each set to improve readability. Similar graphs are in the appendix.

We test our detection technique with four pre-trained models, each pre-trained on a separate dataset, and find our results generalize to a multitude of alternative datasets. Further, we find that our detection technique is robust to a range of adversarial attacks.

To our knowledge, this work is the first to consider the feasibility of broadly detecting all erroneous inputs. Specifically, we find that the model’s internal activations in the softmax layer and final hidden layer are sufficient for automatically filtering incorrectly processed inputs. Figure 2 highlights the separability of correct examples from erroneous examples.

In summary, this paper makes the following contributions:

- This is the first research showing that various erroneous inputs, which neural network models will fail to correctly classify, can be identified using the model’s activations in response to the input.
- We show that several common adversarial perturbations tend to have softmax probabilities distinct from correct examples.
- We achieve state-of-the-art results by considering the activations of both the softmax and final hidden layer of common pre-trained neural networks.

2. Related Work

A variety of research exists on automatically detecting inputs that will cause neural networks to fail. In this section

we discuss the four subfields that compose erroneous inputs as well as the connections of the fields.

Adversarial Attacks Adversarial examples occur when small, meaningful changes to clean data alter a network’s prediction. Szegedy et al. (2014) highlighted these limitations, giving rise to the field of adversarial attacks. Since then, numerous methods have been proposed to generate adversarial attacks (Carlini & Wagner, 2017b; Goodfellow et al., 2015; Moosavi-Dezfooli et al., 2016; Papernot et al., 2015).

Several works have attempted to defend against adversaries (Lu et al., 2017; Metzen et al., 2017), however, the field largely conforms to a classic "white hat"/"black hat" paradigm (i.e., solutions are often temporary because new attacks are created to overcome the defensive solution (Carlini & Wagner, 2017a)). To date, only a few defenses have proven effective on smaller input dimensions (Madry et al., 2019; Schott et al., 2018), making adversarial attacks a significant problem in the field of machine learning.

Researchers have identified the upper bounds of adversarial robustness techniques for certain distributions (Fawzi et al., 2018; Gilmer et al., 2018; Mahloujifar et al., 2018). In particular, Fawzi et al. (2018) suggested a strong relation between adversarial robustness and the linearity of a classifier in latent space. Gilmer et al. (2018) showed that when a model misclassifies even a small fraction of inputs, it can be exposed to adversarial perturbations of size $O(1/\sqrt{n})$, where n is the number of dimensions in the input.

Our work finds that adversarial inputs, generated using a variety of methods (see Section 3.2.4, manifest distinct activation patterns that we use to detect when models will fail. We also consider “natural adversaries,” which categorically overlap with misclassifications.

Image Corruption Deep learning models also perform poorly on corrupted examples. Image corruption is an unintentional, inevitable facet of real-world model deployment: corrupted inputs can range from image quality degradation to lighting changes. For example, autonomous driving models need to be robust to weather and debris (Chaabane et al., 2020; Michaelis et al., 2019). In particular, networks have shown to be susceptible to Gaussian noise, blur, pixelation, and JPEG compression (Dodge & Karam, 2017; Hendrycks & Dietterich, 2019). Some researchers have even proposed that networks should be evaluated on their ability to generalize across such inputs (RichardWebster et al., 2019).

Out-of-Distribution Detection (OOD) An OoD example occurs when a model is presented with data outside of its training paradigm. In this work, OoD examples originate from datasets other than the dataset the baseline model was trained on.

Hendrycks and Dietterich (2018) established a benchmark for OoD detection by using the Maximum Softmax Probability (MSP). Results were presented on several datasets in different neural network modalities such as computer vision and natural language processing. Other works trained neural networks to reject out-of-distribution data with auxiliary branches (DeVries & Taylor, 2018), auxiliary datasets (Hendrycks et al., 2019), GAN examples (Lee et al., 2018), and other train-time techniques (Bevandić et al., 2018; Geifman & El-Yaniv, 2019).

Misclassified Examples and Thresholding Misclassified examples occur when a model is trained on a class of data but the model fails to predict the class successfully on a new input. One technique to detect this poorly-learned data is thresholding. Thresholding has a rich history of research (Chow, 1970; 1957), however, we believe we are the first to consider multiple layers of the network for thresholding.

Hendrycks and Dietterich (2018) provide thresholding results for misclassified examples on contemporary datasets, while (Geifman & El-Yaniv, 2017) presented results of the softmax response from a risk perspective. In recent years, thresholding techniques have been applied to detect adversarial examples (Lu et al., 2017; Pang et al., 2018) and OoD examples (Hendrycks & Gimpel, 2018). Lu et al. (2017) provide the approach most similar to our own. They utilize layers toward the end of deep learning models to detect adversarial examples with SVM-RBF classifiers. Our work shows an ability to detect some adversarial examples using these features; however, we surpass these standards by

considering the hidden layers as well as the softmax layer.

Connecting erroneous inputs Some recent research has found similarities in the above areas. Hendrycks and Gimpel (2018) showed that both misclassified and out-of-distribution examples can be detected by utilizing the maximum softmax probability. Ford et al. (2019) proposed a similarity between the fields of adversarial and corrupted examples, showing empirical and theoretical evidence that these two fields are manifestations of the same phenomena. Another notable cross-domain technique was Liang et al. (2018), who used adversarial perturbations on input data to discriminate in-distribution from OoD examples. Finally, Rozsa and Boulton (2019) argued that adversarial perturbations exist in open space, contrary to popular belief that they exist near training samples.

The above research highlights the distinct work being done in each of these four fields, and previous work that has identified connections between some of these fields. To our knowledge, our work is the first to fully explore the link between all of these areas, and the first to detect them with a single approach.

3. Method

We first formally define the domain of erroneous inputs (Section 3.1) and set up our experimental design (Section 3.2), enumerating the pre-trained models and datasets used in our experiments. Finally, we define our methods for training and testing erroneous input detectors (Section 3.3) and the evaluation metrics used to evaluate our results (Section 3.4).

3.1. Defining the Domain

We defined our domain in the context of detecting when input data to a visual classification model, $f(\mathcal{X}) \rightarrow \mathcal{Y}$, was classified incorrectly. Incorrect classifications in our experiments encompassed out-of-distribution classes (\mathcal{D}_{out}), adversarial examples (\mathcal{A}), corrupted examples (\mathcal{C}), and misclassified in-distribution data (\mathcal{M}). \mathcal{M} could be considered any input from in-domain dataset \mathcal{D}_{in} where output $\mathcal{Y}_{predicted} \neq \mathcal{Y}_{actual}$. In our experiments, we always consider \mathcal{D}_{out} , \mathcal{A} , \mathcal{C} , and \mathcal{M} to belong to the positive class, which were in turn classified against the correctly predicted in-domain dataset \mathcal{D}_{in} where $\mathcal{Y}_{predicted} = \mathcal{Y}_{actual}$.

To build the training set for our binary classifier we use both validation and test sets from the dataset under test. Our training set was built such that $f(\mathcal{A}) \neq \mathcal{Y}_{actual}$ and $f(\mathcal{C}) \neq \mathcal{Y}_{actual}$ — we only used samples which the neural network classified incorrectly. When an adversarial or corrupted example is classified correctly, we do not want to remove the example from the baseline models purview. Adversarial examples were generated from inputs the model originally predicted correctly, i.e. $f(x) = \mathcal{Y}_{actual}$ and $f(x \rightarrow \mathcal{A}) \neq$

\mathcal{Y}_{actual} . Finally, it is implied that $f(\mathcal{D}_{out})$ and $f(\mathcal{M})$ would produce invalid results, so each example will be taken from these datasets.

It should be noted that we did not classify in-domain versus out-of-domain data because we consider the set of everything except \mathcal{D}_{out} to be in-domain: $\{\mathcal{D}_{in}, \mathcal{A}, \mathcal{C}, \mathcal{M}\} \in \mathcal{D}$ while $\mathcal{D}_{out} \notin \mathcal{D}$. Further, our initial experiments were setup to classify correct example sets from each of the erroneous examples sets, i.e. classifying correct examples against the set of misclassified examples. In Section 4.3 we combined the erroneous example sets, and jointly classified the data from correct examples.

3.2. Experimental Setup

For our experiments we used several common baseline datasets and models for image classification. The baseline models were fed various correct data and erroneous data and the activations for both the softmax output and the final hidden layer of the model were collected for use in our detection models. The baseline models were not altered in any way during our experiments.

3.2.1. BASELINE DATASETS AND MODELS

Below are the summaries of the pre-trained models used for each dataset under test. For uniformity, all images passed to the pre-trained models were resized and normalized the same way.

MNIST consists of 60,000 training and 10,000 test examples of 28 x 28 images of handwritten numbers 0 through 9. We trained a simple convolutional neural network with two convolutional layers and two fully connected layers. The model was a standard PyTorch implementation for MNIST classification¹ (LeCun & Cortes, 2010).

CIFAR-10 contains 32 x 32 colored images of 10 different classes of objects (Krizhevsky & Hinton, 2009). The dataset has 50,000 training images and 10,000 testing images. Our CIFAR-10 model was trained using the ResNet50 architecture and open-sourced by (Madry et al., 2019).

Tiny ImageNet is a 200-class subset of the ImageNet dataset where images were cropped and resized to a resolution of 64 x 64. Bounding box information was used in the image cropping (Johnson, 2015). Our Tiny ImageNet model is a pre-trained WideResNet (Zagoruyko & Komodakis, 2017). The trained model was open-sourced by (Hendrycks & Dietterich, 2019).

ImageNet consists of 1000 classes of objects (Russakovsky et al., 2015), with varied dimensions and resolutions. Our work used the validation dataset to produce examples for our detection model. We utilized the default pre-trained

ResNet50 model in the Pytorch library for our ImageNet experiments.

3.2.2. OUT-OF-DISTRIBUTION DATASETS

NotMNIST consists of 28 x 28 black and white images of letters A-J. We fed the images into the MNIST trained model (Bulatov, 2011).

CIFAR-100 contains 32 x 32 colored images of 100 different classes of objects (Krizhevsky & Hinton, 2009). We filtered out classes similar to those found in CIFAR-10 to ensure all classes were truly OoD, leaving 74 classes. Details on excluded classes are in the appendix.

The Scene Understanding dataset (SUN) contains images of scenes with varying resolutions (Xiao et al., 2010).

Places365 contains 365 classes of scenes with varying image resolutions. We use the high-resolution validation set for use in our Tiny ImageNet and ImageNet models (Zhou et al., 2018).

ImageNet-O dataset was constructed from sampled images from ImageNet-22K (Hendrycks et al., 2020). First, images overlapping with classes in ImageNet-1K were filtered out. Next, they retained images that a ResNet50 ImageNet-1K model classified with high softmax probability. Finally, they hand-selected a subset of high-quality images.

3.2.3. CORRUPTION DATASETS

CIFAR-10-C, Tiny ImageNet-C, ImageNet-C are image corruption datasets for the purpose of testing model robustness (Hendrycks & Dietterich, 2019). Each corrupted dataset included 15 common visual corruptions such as Gaussian noise, blur, and digital distortions. Each type of corruption had five levels of 'severity' for a total of 75 distinct corruptions per image. We used each corruption and severity type in our models. We fed Gaussian noise to the MNIST model to simulate corruption.

3.2.4. ADVERSARIAL ATTACK METHODS

White-box attacks methods are used to generate adversarial examples. White-box methods assume the attacker has full access to the learning model.

Fast Gradient Sign Method (FGSM) was an attack introduced by Goodfellow et al. (2015). It adjusts the inputs to maximize the loss based on the back-propagated gradients of the predicted value: $f(\mathcal{A}) = \mathcal{X} + \epsilon \text{sign}(\nabla_{\mathcal{X}} J(\theta, \mathcal{X}, \mathcal{Y}))$. FGSM examples were generated using $\epsilon=0.01$.

Carlini and Wagner l_2 Attack (C & W l_2) searches for low distortion in the l_2 metric (Carlini & Wagner, 2017b). L_2 attacks measure the Euclidean distance between the original and the perturbed examples, equal to the root mean

¹<https://github.com/pytorch/examples/tree/master/mnist>

Table 1. MNIST and CIFAR-10 experiments for Maximum Softmax Probability (MSP), Sorted Softmax, and Final Hidden Vector classification. Full results in appendix. The detail column highlights the dataset or method used for the specific domain.

MNIST		MSP		SORTED SOFTMAX		HIDDEN ACTIVATIONS	
TEST TYPE	DETAIL	AUROC	AUPR	AUROC	AUPR	AUROC	AUPR
MISCLASSIFIED	-	.985	.971	.986	.979	1.00	1.00
OUT-OF-DISTRIBUTION	NOTMNIST	.922	.923	.922	.924	1.00	1.00
CORRUPTION	GAUSSIAN NOISE	.985	.980	.987	.983	1.00	1.00
ADVERSARIAL	FGSM ($\epsilon = 0.3$)	.999	.998	.999	.999	1.00	1.00
CIFAR-10							
MISCLASSIFIED	-	.926	.902	.925	.900	.750	.724
OUT-OF-DISTRIBUTION	SUN	.915	.900	.926	.918	.913	.909
CORRUPTION	CIFAR-10-C	.958	.946	.959	.949	.855	.855
ADVERSARIAL	PGD	.997	.994	.999	.999	1.00	1.00
ADVERSARIAL	C & W l_∞	.755	.700	.780	.770	1.00	1.00
ADVERSARIAL	C & W l_2	.934	.890	.964	.965	1.00	1.00

squared difference. Notable in the Carlini and Wagner attacks is κ , which allows a confidence level for the adversarial example to be calibrated. This means examples can be generated that the neural network predicts incorrectly with high probability. Examples in our main experiments were generated with $\kappa = 0$ — we did not search for a perturbed input which satisfied a specific confidence.

Carlini and Wagner l_∞ Attack (C & W l_∞) was a modified version of the C&W l_2 attack. It controls the l_∞ norm, i.e. the maximum perturbation applied to any pixel (Carlini & Wagner, 2017b).

Projected Gradient Descent (PGD) finds the perturbation that maximizes the loss of a model on an input, and, after each iteration, it projects the perturbation onto an l_p ball of radius ϵ while also clipping values so they fall within a permitted range (Madry et al., 2019).

Carlini and Wagner l_2 , l_∞ attacks and PGD attack examples were generated using the adversarial-robustness-toolbox with default parameters (Nicolae et al., 2018). We used the PyTorch implementation of the FGSM attack.

ImageNet-A is a dataset of ‘natural adversaries’. ImageNet-A was created by taking examples from the ImageNet dataset and removing examples the model predicted correctly. Then, a subset of high-quality images were hand-selected (Hendrycks et al., 2020). We included this dataset as an extension to our misclassified experiments.

3.3. Detection Model

We employed a linear Support Vector Machine (SVM) classifier for our experiments, where examples ($\{x_1\}$, y_1), ..., ($\{x_n\}$, y_n) were trained to maximize the hyperplane be-

tween the groups $y=0$ and $y=1$.

We followed the training and evaluation standards of Hendrycks and Gimpel (2018) to evaluate our detection model. Specifically, we fit and evaluate the model on the same data to enable baseline calculations for Maximum Softmax Probability (MSP) and to calculate threshold independent AUROC and AUPR metrics. In the appendix, we also validated our methods with both five-fold cross-validation and the optimal SVM hyperplane. Our results were consistent across all evaluation techniques.

To generate features $\{x_1\} \dots \{x_n\}$ for our sorted softmax vector model, we take all values from the softmax output vector and sort them from smallest to largest. Our hidden activation vector model utilizes the second to last layer of all baseline models, which is a fully-connected layer. For ResNet50 models, this is a vector of 2048 values. For the WideResNet model the vector is 128 values. Our combined model uses the hidden activation vector with the sorted softmax vector appended.

We present results in this paper with a balanced dataset: each model contains the same number of correct and erroneous examples. However, to better simulate real-world scenarios we use varying ratios of examples (see appendix). For example, (Hendrycks et al., 2019) tested their Outlier Exposure using a ratio of 5:1 for D_{in} to D_{out} . Our results for a 5:1 ratio are in the appendix. We could not find existing research with results for specific sets of adversarial or corrupted examples.

Table 2. Tiny ImageNet and ImageNet experiments for MSP, Sorted Softmax, and hidden activation vector classification. Full results in appendix.

TINY IMAGENET		MSP		SORTED SOFTMAX		HIDDEN ACTIVATIONS	
TEST TYPE	DETAIL	AUROC	AUPR	AUROC	AUPR	AUROC	AUPR
MISCLASSIFIED	-	.929	.909	.929	.910	.720	.695
OUT-OF-DISTRIBUTION	PLACES365	.909	.902	.912	.904	.988	.987
CORRUPTION	TINY IMAGENET-C	.906	.898	.908	.899	.966	.964
ADVERSARIAL	FGSM ($\epsilon = 0.01$)	.898	.889	.902	.893	.999	.999
ADVERSARIAL	PGD	.991	.992	.991	.993	1.00	1.00
ADVERSARIAL	C & W l_2	.933	.867	.982	.980	.570	.550
ADVERSARIAL	C & W l_∞	.885	.818	.920	.900	.600	.570
IMAGENET							
MISCLASSIFIED	-	.857	.837	.862	.840	.908	.907
OUT-OF-DISTRIBUTION	SUN	.832	.827	.837	.832	.998	.998
OUT-OF-DISTRIBUTION	PLACES365	.849	.845	.852	.847	1.00	1.00
OUT-OF-DISTRIBUTION	IMAGENET-O	.675	.570	.680	.580	1.00	1.00
CORRUPTION	IMAGENET-C (NOISE)	.924	.922	.924	.919	1.00	1.00
NAT. ADVERSARIAL	IMAGENET-A	.910	.909	.911	.913	.976	.977
ADVERSARIAL	PGD	.990	.990	.990	.990	1.00	1.00
ADVERSARIAL	C & W l_∞	.870	.800	.915	.883	.804	.808
ADVERSARIAL	C & W l_2	.890	.810	.966	.954	.772	.763

3.4. Testing and Evaluation Metrics

We evaluate binary detection tasks using three metrics: area under the receiver operating characteristic curve (AUROC) and area under the precision-recall curve (AUPR), and false positive rate at N% true positive rate (FPR_N).

AUROC plots the true positive rate (TPR) against the false positive rate (FPR). Random classifiers score 50% while perfect classifiers achieve 100%. The metric works by varying threshold values in a binary predictor and is thus threshold-independent. To ensure threshold-independent metrics in our models, we use the decision function to the SVM hyperplane, which predicts confidence for each examples based on its signed distance to the hyperplane.

AUPR is another cumulative distribution function which plots the precision (True Positive)/(True Positive + False Positive) versus the recall (True Positive)/(True Positive + False Negative). This metric is more informative when the number of positive examples varies greatly from the number of negative examples.

For our combined model we also present FPR_N scores, also used by (Hendrycks et al., 2019; Liang et al., 2018; Liu et al., 2018). The FPR_N calculates the false positive rate at a set True Positive Rate. In other words, we calculate the probability that the model fires a false alarm given a

set detection rate. We use TPR of 95%, similar to past papers. Detecting a high percentage of erroneous inputs with relatively few false alarms is useful in any real-world scenario.

4. Results

In this section we present the truncated results of tables 1, 2, and 3. Full results are in the appendix.

4.1. Sorted Softmax and Hidden Activation Models

In Tables 1 and 2 we directly compared the applicability of our two detection models with Hendrycks and Gimpel’s (2018) Maximum Softmax Probability (MSP). On average, both of the proposed methods performed better than MSP. However, in the Table 1 CIFAR-10 experiments, C & W l_∞ adversarial examples were difficult to separate with both MSP and Sorted Softmax (AUROC 0.755, AUPR 0.700; AUROC 0.780, AUPR 0.770, respectively), but could be easily separated with the hidden activations. Inversely, the hidden activations model struggled to separate corrupted, misclassified, and out-of-distribution inputs as well as either sorted softmax or MSP. The more complex models in Table 2 showed different separation patterns, most notably, reversing the results from C & W l_∞ .

Table 3. CIFAR-10, Tiny ImageNet, and ImageNet experiments for our combined model. Up arrows represent a higher score being better, while down arrows indicate a lower score is better. See appendix for all experimental results.

TEST TYPE	HIDDEN ACTIVATIONS + SORTED SOFTMAX		
	AUROC \uparrow	AUPR \uparrow	FPR (95%) \downarrow
CIFAR-10			
SUN	.964	.961	.162
CIFAR-10-C	.973	.968	.106
FGSM	.930	.906	.190
C & W l_∞	1.00	1.00	.000
PGD	1.00	1.00	.000
TINY IMAGENET			
MISCLASSIFIED	.932	.913	.237
SUN	.996	.996	.018
PLACES365	.995	.994	.023
CORRUPTED	.984	.984	.075
PGD	.100	.100	.000
C & W l_2	.986	.985	.059
IMAGENET			
MISCLASSIFIEDD	.984	.985	.100
SUN	1.00	1.00	.000
PLACES365	1.00	1.00	.000
IMAGENET-C	1.00	1.00	.000
IMAGENET-O	1.00	1.00	.000
IMAGENET-A	.995	.995	.027
FGSM	1.00	1.00	0.00
C & W l_∞	.993	.993	.029
C & W l_2	1.00	1.00	0.00
PGD	1.00	1.00	0.00

These findings had two important indications. First, there was strong evidence that the broad range of erroneous inputs were linked and could be jointly detected. Second, sorted softmax and hidden activations performed better than the MSP baseline, but the success of each method varied across models and erroneous inputs. In Section 4.2, we overcome these limitations with a combined model.

4.2. Combined Model

We combined the sorted softmax and hidden activations features into a single model to detect faulty data. Since the success of each method varied depending on the model and erroneous input (Section 4.1), we hypothesized that combining the features would result in a more consistent

method that could identify all erroneous inputs, regardless of model. Experiments were performed on CIFAR-10, Tiny ImageNet and ImageNet datasets — the same faulty data types examined in Section 4.1.

Table 3 highlights the average AUPR, AUROC, and FPR/V for each experiment. Across all of the experiments, the combined model surpassed the performance of the methods in Section 4.1. The lowest performance of the combined model varied; 0.930 AUROC for FGSM inputs with the CIFAR-10 model, 0.925 AUROC for C & W l_∞ with the Tiny ImageNet model, and 0.984 for misclassified with the ImageNet model.

In particular, the combined features from ImageNet allowed nearly perfect classification. One possible explanation could be that the ImageNet model generated 3048 total features for the SVM while the WideResNet only provided 328, indicating that models with more linear activation features allow easier classification between correct and erroneous examples.

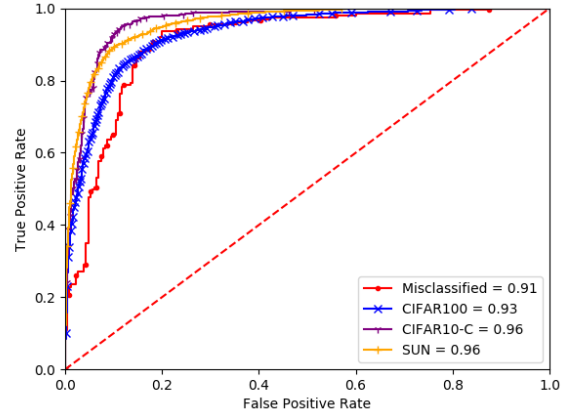


Figure 3. CIFAR-10 AUROC for several data types classified against correct predictions with the combined model.

4.3. Combined Datasets

We investigated the possibility of a single model that could identify all erroneous inputs. Specifically, we classified the erroneous inputs from correctly predicted examples \mathcal{D}_{in} using the combined feature sets (Section 4.2). Erroneous inputs were randomly sampled from the set of all erroneous inputs to create a balanced dataset, i.e. $\{\mathcal{D}_{out}, \mathcal{A}, \mathcal{C}, \mathcal{M}\}$ (see appendix for details). We consider the effects of unbalanced datasets in Section 4.3.2 and in the appendix.

In Table 4, we present the classification results on the combined datasets. We found that, across all of our models, erroneous inputs could be detected with high performance (AUROCs between 0.953 and 0.999). In the appendix, we

Table 4. Results when we randomly sample inputs from each erroneous dataset, excluding PGD attacks and ImageNet-O. ImageNet includes results for each domain except PGD and ImageNet-O, ImageNet+ includes only PGD and ImageNet-O. Experiments are performed on balanced data and averaged across ten experiments. Standard deviation is included for each metric.

BASE DATASET	AUROC \uparrow	AUPR \uparrow	FPR(95%) \downarrow
MNIST	.999 \pm .0002	.999 \pm .0001	.007 \pm .0001
CIFAR-10	.953 \pm .0001	.954 \pm .0008	.256 \pm .0012
TINY IMAGENET	.953 \pm .0004	.952 \pm .0004	.272 \pm .0004
IMAGENET-	.970 \pm .0014	.971 \pm .0014	.198 \pm .0110
IMAGENET+	.998 \pm .0003	.998 \pm .0003	.005 \pm .0001

also present the results for MSP, the baseline method we compare against, and find that our combined model vastly outperforms the MSP baseline.

A manual analysis of model failures found that PGD attacks and ImageNet-O were consistently not detected by our model because their maximum softmax probabilities tended to be higher (PGD inputs had nearly 100% probability on average; ImageNet-O had an average probability of 93%) than for correctly classified examples (80% average for ImageNet, 86% for Tiny ImageNet). All other erroneous example sets were lower (between 25% and 55% average). Because we only used linear SVMs, it was impossible for our models to correctly filter both cases.

4.3.1. HIGH CONFIDENCE ADVERSARIAL ATTACKS

We explored the limits of our models’ ability to filter adversarial inputs. Specifically, we generated high confidence adversarial examples to bypass our MNIST detection model using Carlini and Wagner l_∞ and l_2 attacks. We generated 270 adversarial examples with an average confidence of 99.9%, compared to 99.5% for correctly learned examples. When tested, our model scores an AUROC of .995 and AUPR of .995, while MSP had an AUROC of .832 and an AUPR of .708. These experiments highlighted a distinct benefit of our model over the MSP baseline. However, we note that we did not exhaustively test every adversarial attack and that other attacks may fool our technique.

4.3.2. IMBALANCED DATASETS

Building upon the experiments in Section 4.3.1, we also explored how our model performed when the datasets were heavily imbalanced. Testing the full set of 9903 correct examples against 270 adversarial examples, our model scored .926 and .460 for AUROC and AUPR, respectively. This was a strong improvement over MSP, which scored .802 and .058, but it highlighted the limitations of our model with

imbalanced data.

5. Discussion

Erroneous inputs have been largely studied as distinct phenomenon, with the detection of different faulty inputs requiring their own methods. Our experimental results show that these faulty inputs can be broadly detected by considering a model’s internal behavior. Furthermore, these patterns are distinct enough that they are linearly separable. We propose a new internal activation combination that allows for the broad detection of erroneous inputs, and establish standards for the detection of faulty data including adversarial, corrupted, out-of-distribution, and misclassified examples. A substantial benefit to this approach is that it requires no special training or modification to the baseline model. Apart from Hendrycks and Gimpel (2018), most work in the area requires some sort of network modification during training or test time.

Despite this, there are limitations to our approach that future research will need to address; first, the current research focuses on the image domain. It remains to be seen how well this technique will generalize to other domains (like natural language processing), but initial work by Hendrycks and Gimpel (2018) found MSP, which our method directly builds on, was useful in several other domains, indicating our techniques will likely generalize. Second, our detection technique is vulnerable when presented with heavily imbalanced data (Section 4.3.2). However, given that our method requires erroneous detection models to be built for individual models, from activation data from those models, dataset imbalance is trivial to address in the data collection process. Third, we limit our erroneous detection models to linear SVMs, which are incapable of more complicated classifications. Predictably, these models fail when testing for multiple erroneous inputs – for example, PGD examples we generated led to higher maximum softmax probability, while other adversarial inputs caused lower maximum softmax probability. Nonetheless, our models were highly successful at detecting erroneous inputs, and the simplicity of our model has important implications for real-time usage.

A single deep learning model capable of understanding any input is years away at best, and thus detection of ‘bad’ data, which will cause models to fail, is essential for the safe use of any real-world system. We argue that, by moving towards detection of any non-learned data in broader application of a learning based system, we can progress the effective deployment of machine learning models in real-world applications.

References

Amodei, D., Olah, C., Steinhardt, J., Christiano, P., Schulman, J., and Man, D. Concrete problems in AI safety.

- arXiv:1606.06565*, 2016. URL <http://arxiv.org/abs/1606.06565>.
- Bendale, A. and Boulton, T. Towards open set deep networks. *arXiv:1511.06233 [cs]*, 2015.
- Bevandić, P., Krešo, I., Oršić, M., and Šegvić, S. Discriminative out-of-distribution detection for semantic segmentation. *arXiv preprint arXiv:1808.07703*, 2018.
- Bulatov, Y. notMNIST. 2011.
- Carlini, N. and Wagner, D. Adversarial examples are not easily detected: Bypassing ten detection methods. *arXiv:1705.07263 [cs]*, 2017a.
- Carlini, N. and Wagner, D. Towards evaluating the robustness of neural networks. *arXiv:1608.04644 [cs]*, 2017b.
- Chaabane, M., Trabelsi, A., Blanchard, N., and Beveridge, R. Looking ahead: Anticipating pedestrians crossing with future frames prediction. In *2020 IEEE Winter Conference on Applications of Computer Vision (WACV)*. IEEE, 2020.
- Chow, C. An Optimum Recognition Error and Reject Trade-off. 1970.
- Chow, C. K. An optimum character recognition system using decision functions. *IRE Transactions on Electronic Computers*, EC-6(4):247–254, 1957. ISSN 0367-9950. doi: 10.1109/TEC.1957.5222035.
- DeVries, T. and Taylor, G. W. Learning confidence for out-of-distribution detection in neural networks. *arXiv:1802.04865 [cs, stat]*, 2018.
- Dodge, S. and Karam, L. A study and comparison of human and deep learning recognition performance under visual distortions. *arXiv:1705.02498 [cs]*, 2017.
- Fawzi, A., Fawzi, H., and Fawzi, O. Adversarial vulnerability for any classifier. *arXiv:1802.08686 [cs, stat]*, 2018.
- Ford, N., Gilmer, J., Carlini, N., and Cubuk, D. Adversarial examples are a natural consequence of test error in noise. *arXiv:1901.10513 [cs, stat]*, 2019.
- Geifman, Y. and El-Yaniv, R. Selective classification for deep neural networks. *arXiv:1705.08500 [cs]*, 2017.
- Geifman, Y. and El-Yaniv, R. SelectiveNet: A deep neural network with an integrated reject option. *arXiv:1901.09192 [cs, stat]*, 2019.
- Geirhos, R., Temme, C. R. M., Rauber, J., Schütt, H. H., Bethge, M., and Wichmann, F. A. Generalisation in humans and deep neural networks. In Bengio, S., Wallach,
- H., Larochelle, H., Grauman, K., Cesa-Bianchi, N., and Garnett, R. (eds.), *Advances in Neural Information Processing Systems 31*, pp. 7538–7550. Curran Associates, Inc., 2018.
- Gilmer, J., Metz, L., Faghri, F., Schoenholz, S. S., Raghu, M., Wattenberg, M., and Goodfellow, I. Adversarial spheres. *arXiv:1801.02774 [cs]*, 2018.
- Goodfellow, I. J., Shlens, J., and Szegedy, C. Explaining and harnessing adversarial examples. *arXiv:1412.6572 [cs, stat]*, 2015.
- Hendrycks, D. and Dietterich, T. Benchmarking neural network robustness to common corruptions and perturbations. *arXiv:1903.12261 [cs, stat]*, 2019.
- Hendrycks, D. and Gimpel, K. A baseline for detecting misclassified and out-of-distribution examples in neural networks. *arXiv:1610.02136 [cs]*, 2018.
- Hendrycks, D., Mazeika, M., and Dietterich, T. Deep anomaly detection with outlier exposure. *arXiv:1812.04606 [cs, stat]*, 2019.
- Hendrycks, D., Zhao, K., Basart, S., Steinhardt, J., and Song, D. Natural adversarial examples. *arXiv:1907.07174 [cs, stat]*, 2020.
- Johnson, S. Tiny imagenet visual recognition challenge. pp. 211–252, 2015. URL <https://tiny-imagenet.herokuapp.com/>.
- Krizhevsky, A. and Hinton, G. Learning multiple layers of features from tiny images. pp. 211–252, 2009.
- LeCun, Y. and Cortes, C. MNIST handwritten digit database. 2010. URL <http://yann.lecun.com/exdb/mnist/>.
- Lee, K., Lee, H., Lee, K., and Shin, J. Training confidence-calibrated classifiers for detecting out-of-distribution samples. *arXiv:1711.09325 [cs, stat]*, 2018.
- Liang, S., Li, Y., and Srikant, R. Enhancing the reliability of out-of-distribution image detection in neural networks. *arXiv:1706.02690 [cs, stat]*, 2018.
- Liu, S., Garrepalli, R., Dietterich, T. G., Fern, A., and Hendrycks, D. Open category detection with PAC guarantees. *arXiv:1808.00529 [cs, stat]*, 2018.
- Lu, J., Issararanon, T., and Forsyth, D. SafetyNet: Detecting and rejecting adversarial examples robustly. *arXiv:1704.00103 [cs]*, 2017.
- Madry, A., Makelov, A., Schmidt, L., Tsipras, D., and Vladu, A. Towards deep learning models resistant to adversarial attacks. *arXiv:1706.06083 [cs, stat]*, 2019.

- Mahloujifar, S., Diochnos, D. I., and Mahmood, M. The curse of concentration in robust learning: Evasion and poisoning attacks from concentration of measure. *arXiv:1809.03063 [cs, stat]*, 2018.
- Metzen, J. H., Genewein, T., Fischer, V., and Bischoff, B. On detecting adversarial perturbations. *arXiv:1702.04267 [cs, stat]*, 2017.
- Michaelis, C., Mitzkus, B., Geirhos, R., Rusak, E., Bringmann, O., Ecker, A. S., Bethge, M., and Brendel, W. Benchmarking robustness in object detection: Autonomous driving when winter is coming. *arXiv:1907.07484 [cs, stat]*, 2019.
- Moosavi-Dezfooli, S.-M., Fawzi, A., and Frossard, P. DeepFool: a simple and accurate method to fool deep neural networks. *arXiv:1511.04599 [cs]*, 2016.
- Nicolae, M.-I., Sinn, M., Tran, M. N., Buesser, B., Rawat, A., Wistuba, M., Zantedeschi, V., Baracaldo, N., Chen, B., Ludwig, H., Molloy, I., and Edwards, B. Adversarial robustness toolbox v1.0.1. *CoRR*, 1807.01069, 2018. URL <https://arxiv.org/pdf/1807.01069>.
- Pang, T., Du, C., Dong, Y., and Zhu, J. Towards robust detection of adversarial examples. In Bengio, S., Wallach, H., Larochelle, H., Grauman, K., Cesa-Bianchi, N., and Garnett, R. (eds.), *Advances in Neural Information Processing Systems 31*, pp. 4579–4589. Curran Associates, Inc., 2018.
- Papernot, N., McDaniel, P., Jha, S., Fredrikson, M., Celik, Z. B., and Swami, A. The limitations of deep learning in adversarial settings. *arXiv:1511.07528 [cs, stat]*, 2015.
- RichardWebster, B., Anthony, S. E., and Scheirer, W. J. Psyphy: A psychophysics driven evaluation framework for visual recognition. *IEEE Transactions on Pattern Analysis and Machine Intelligence (T-PAMI)*, 41(9), September 2019.
- Rozsa, A. and Boulton, T. E. Improved adversarial robustness by reducing open space risk via tent activations. *arXiv:1908.02435 [cs]*, 2019.
- Russakovsky, O., Deng, J., Su, H., Krause, J., Satheesh, S., Ma, S., Huang, Z., Karpathy, A., Khosla, A., Bernstein, M., Berg, A. C., and Fei-Fei, L. ImageNet Large Scale Visual Recognition Challenge. *International Journal of Computer Vision (IJCV)*, 115(3):211–252, 2015. doi: 10.1007/s11263-015-0816-y.
- Scheirer, W., Rocha, A., Sapkota, A., and Boulton, T. Toward open set recognition. *IEEE transactions on pattern analysis and machine intelligence*, 35:1757–72, 07 2013. doi: 10.1109/TPAMI.2012.256.
- Schott, L., Rauber, J., Bethge, M., and Brendel, W. Towards the first adversarially robust neural network model on mnist. pp. 16, 2018.
- Szegedy, C., Zaremba, W., Sutskever, I., Bruna, J., Erhan, D., Goodfellow, I., and Fergus, R. Intriguing properties of neural networks. *arXiv:1312.6199 [cs]*, 2014.
- Xiao, J., Hays, J., Ehinger, K. A., Oliva, A., and Torralba, A. SUN database: Large-scale scene recognition from abbey to zoo. In *2010 IEEE Computer Society Conference on Computer Vision and Pattern Recognition*, pp. 3485–3492. IEEE, 2010. ISBN 978-1-4244-6984-0. doi: 10.1109/CVPR.2010.5539970.
- Zagoruyko, S. and Komodakis, N. Wide residual networks. *arXiv:1605.07146 [cs]*, 2017.
- Zhou, B., Lapedriza, A., Khosla, A., Oliva, A., and Torralba, A. Places: A 10 million image database for scene recognition. *IEEE Transactions on Pattern Analysis and Machine Intelligence*, 40(6):1452–1464, 2018. ISSN 0162-8828, 2160-9292. doi: 10.1109/TPAMI.2017.2723009.